THE JOURNAL OF BIOLOGICAL CHEMISTRY
Vol. 275, No. 8, Issue of February 25, pp. 5329–5336, 2000

Printed in U.S.A.

Poliovirus RNA-dependent RNA Polymerase ($3D^{pol}$)

ASSEMBLY OF STABLE, ELONGATION-COMPETENT COMPLEXES BY USING A SYMMETRICAL PRIMER-TEMPLATE SUBSTRATE (sym/sub)*

(Received for publication, August 12, 1999, and in revised form, December 5, 1999)

Jamie J. Arnold and Craig E. Cameron‡

From the Department of Biochemistry and Molecular Biology, Pennsylvania State University, University Park, Pennsylvania 16802

Detailed studies of the kinetics and mechanism of nucleotide incorporation catalyzed by the RNA-dependent RNA polymerase from poliovirus, $3D^{pol}$, have been limited by the inability to assemble elongation complexes that permit activity to be monitored by extension of end-labeled primers. We have solved this problem by employing a short, symmetrical, heteropolymeric RNA primer-template that we refer to as "sym/sub." Formation of $3D^{pol}$-sym/sub complexes is slow owing to a slow rate of association (0.1 μM^{-1} s^{-1}) of $3D^{pol}$ and sym/sub and a slow isomerization (0.076 s^{-1}) of the $3D^{pol}$-sym/sub complex that is a prerequisite for catalytic competence of this complex. Complex assembly is stoichiometric under conditions in which competing reactions, such as enzyme inactivation, are eliminated. Inactivation of $3D^{pol}$ occurs at a maximal rate of 0.051 s^{-1} at 22 °C in reaction buffer lacking nucleotide. At this temperature, ATP protects $3D^{pol}$ against inactivation with a $K_{0.5}$ of 37 μM. Once formed, $3D^{pol}$-sym/sub elongation complexes are stable ($t_{1/2}$ = 2 h at 22 °C) and appear to contain only a single polymerase monomer. In the presence of Mg^{2+}, AMP, 2′-dAMP, and 3′-dAMP are incorporated into sym/sub by $3D^{pol}$ at rates of 72, 0.6, and 1 s^{-1}, respectively. After incorporation of AMP, $3D^{pol}$-sym/sub product complexes have a half-life of 8 h at 22 °C. The stability of $3D^{pol}$-sym/sub complexes is temperature-dependent. At 30 °C, there is a 2–8-fold decrease in complex stability. Complex dissociation is the rate-limiting step for primer utilization. $3D^{pol}$ dissociates from the end of template at a rate 10-fold faster than from internal positions. The sym/sub system will facilitate mechanistic analysis of $3D^{pol}$ and permit a direct kinetic and thermodynamic comparison of the RNA-dependent RNA polymerase to the other classes of nucleic acid polymerases.

Critical to the multiplication of all viruses are transcription and replication of the viral genome. In the case of positive-strand RNA viruses, these processes are catalyzed by the virus-encoded RNA-dependent RNA polymerase (RdRP).[1] Specific inhibitors of the RdRP should serve as potent antiviral agents. Indeed, inhibitors of viral DNA polymerases and reverse transcriptase (RT) are used clinically to treat infection by herpesviruses and human immunodeficiency virus (1, 2). Of course, cellular polymerases are also potential targets for antiviral chemotherapeutics that inhibit viral polymerases. Therefore, target specificity is of central importance to the development of clinically useful compounds. In some cases, drug activation only occurs in virus-infected cells thereby increasing specificity and diminishing toxicity (1). In others, however, infected cell-specific, activation mechanisms are not an option, and other approaches are required (2).

A comprehensive understanding of the differences between viral and cellular polymerases facilitates the design of specific inhibitors. In the case of human immunodeficiency virus RT, a combination of detailed kinetic (3–12) and structural (13–18) information was essential to provide an understanding of the molecular basis for RT function and the mechanism of action of non-nucleoside inhibitors of RT (9, 10). In fact, a description of the nucleotide addition cycle catalyzed by all classes of polymerases studied to date has benefited from both kinetic and structural analyses (19–28). The "structural era" for the RdRP has begun with the recent solution of the x-ray crystal structure for the RdRP from poliovirus, $3D^{pol}$ (29). For this reason, poliovirus $3D^{pol}$ is the ideal model system to use in the study of RdRP function. Unfortunately, detailed, mechanistic information regarding $3D^{pol}$-catalyzed nucleotide incorporation is sparse. The existing gap derives from the inability to assemble stoichiometrically $3D^{pol}$-primer-template complexes that permit nucleotide incorporation to be followed by extension of end-labeled primers.

Previous studies of $3D^{pol}$-catalyzed nucleotide incorporation that utilized short, heteropolymeric RNA primer-templates as substrates demonstrated that this enzyme binds to primer-template such that some enzyme has the 3′-OH from the "primer" strand in the catalytic center ("correct" orientation) and some enzyme has the 3′-OH from the "template" strand in the catalytic center ("incorrect" orientation) (30). When bound in the "incorrect" orientation, $3D^{pol}$ adds non-templated nucleotides to the blunt end of primer-template (30). Of course, heterogeneous binding of $3D^{pol}$ to primer-template further complicates mechanistic analysis of this enzyme. In this report, we demonstrate that the use of a symmetrical primer-template substrate (sym/sub) permits the assembly of stable, elongation-competent $3D^{pol}$-primer-template complexes. The sym/sub system will facilitate quantitative analysis of the kinetics and mechanism of $3D^{pol}$-catalyzed nucleotide incorporation.

EXPERIMENTAL PROCEDURES

Materials—[γ-^{32}P]ATP (>7,000 Ci/mmol) was from ICN; nucleoside 5′-triphosphates, 2′-deoxynucleoside 5′-triphosphates, and 2′,3′-dideoxynucleoside 5′-triphosphates (all nucleotides were ultrapure solutions) were from Amersham Pharmacia Biotech; 3′-deoxyadenosine 5′-triphosphate (cordycepin) was from Sigma; all RNA oligonucleotides

* This work was supported in part by Howard Temin Award CA75118 from the NCI and NIAID Grant AI45818 from the National Institutes of Health (both to C. E. C.). The costs of publication of this article were defrayed in part by the payment of page charges. This article must therefore be hereby marked "*advertisement*" in accordance with 18 U.S.C. Section 1734 solely to indicate this fact.

‡ To whom correspondence should be addressed. Tel.: 814-863-8705; Fax: 814-863-7024; E-mail: cec9@psu.edu.

[1] The abbreviations used are: RdRP, RNA-dependent RNA polymerase; PAGE, polyacrylamide gel electrophoresis; nt, nucleotide; NTP, nucleoside-5′-triphosphate; dNTP, 2′-deoxynucleoside-5′-triphosphate; ddNTP, 2′,3′-dideoxynucleoside-5′-triphosphate; NMP, nucleoside-5′-monophosphate; dNMP, 2′-deoxynucleoside-5′-monophosphate; ddNMP, 2′,3′-dideoxynucleoside-5′-monophosphate; RT, reverse transcriptase.

were from Dharmacon Research, Inc. (Boulder, CO); T4 polynucleotide kinase was from New England Biolabs, Inc.; All other reagents were of the highest grade available from Sigma or Fisher.

Expression and Purification of 3D^{pol}—Expression and purification of 3D^{pol} were performed as described previously (31).

Purification of sym/sub—The RNA oligonucleotide was purified by denaturing PAGE. Gels consisted of 21.3% acrylamide, 1.7% bisacrylamide, 7 M urea, and 1× TBE (89 mM Tris base, 89 mM boric acid, and 2 mM EDTA). The oligonucleotide ladder was visualized by UV shadowing. A gel slice containing only the full-length oligonucleotide was removed, and the nucleic acid was electroeluted from the gel in 1× TBE by using an Elutrap apparatus (Schleicher & Schuell). Oligonucleotides were desalted on Sep-Pak columns (Millipore) as specified by the manufacturer. Oligonucleotides were hydrolyzed to remove the 2′-OH protecting groups as specified by the manufacturer. The concentrated, hydrolyzed RNA stocks (typically 1 mM) contained 330 mM Tris acetate, pH 7.0. Oligonucleotides were diluted in $T_{10}E_1$ (10 mM Tris, 1 mM EDTA, pH 8.0), to the indicated concentrations. Oligonucleotides were stored at −80 °C until use. Concentrations were determined by measuring the absorbance at 260 nm in 50 mM K_2PO_4, pH 7.0, 6 M guanidine by using a calculated extinction coefficient of 101,600 M^{-1} cm^{-1} (32).

5′-^{32}P Labeling of sym/sub—The RNA oligonucleotide was end-labeled by using [γ-^{32}P]ATP and T4 polynucleotide kinase from New England Biolabs essentially as specified by the manufacturer. Reactions, typically 30 μl, contained 11 μM [γ-^{32}P]ATP, 10 μM RNA oligonucleotide (sym/sub), 1× Kinase Buffer and 0.4 units/μl T4 polynucleotide kinase. Reactions were incubated at 37 °C for 60 min. Unincorporated nucleotide was removed by passing the sample over two consecutive 1-ml Sephadex G-25 (Sigma) spun columns. We assumed the concentration of end-labeled RNA remained constant.

Annealing of sym/sub—1 μM end-labeled sym/sub was mixed with 99 μM unlabeled sym/sub in $T_{10}E_1$, pH 8.0, and heated to 90 °C for 1 min and slowly cooled to 10 °C at a rate of approximately 5 °C/min in a Progene Thermocycler.

3D^{pol} Assays—Reactions contained 50 mM HEPES, pH 7.5, 10 mM 2-mercaptoethanol, 5 mM $MgCl_2$, 60 μM $ZnCl_2$, 500 μM NTP, sym/sub, and 3D^{pol}. Reactions were quenched by addition of EDTA to a final concentration of 50 mM. Specific concentrations of primer-template and 3D^{pol}, along with any deviations from the above, are indicated in the appropriate figure legend. 3D^{pol} was diluted immediately prior to use in 50 mM HEPES, pH 7.5, 10 mM 2-mercaptoethanol, 60 μM $ZnCl_2$, and 20% glycerol. The volume of enzyme added to any reaction was always less than or equal to one-tenth the total volume.

Rapid Chemical Quench-flow Experiments—Rapid mixing/quenching experiments were performed by using a model RQF-3 chemical quench-flow apparatus (KinTek Corp., State College, PA). Experiments were performed at 30 °C by using a circulating water bath. 3D^{pol}-sym/sub complex in 50 mM HEPES, pH 7.5, 10 mM 2-mercaptoethanol, 60 μM $ZnCl_2$, and 5 mM $MgCl_2$ was rapidly mixed with the nucleotide substrate in 50 mM HEPES, pH 7.5, 10 mM 2-mercaptoethanol, 60 μM $ZnCl_2$, and 5 mM $MgCl_2$, and the reactions were quenched by addition of 0.5 M EDTA to a final concentration of 0.3 M.

Product Analysis, Denaturing PAGE—An equal volume of loading buffer, 10 μl (90% formamide, 0.025% bromphenol blue, and 0.025% xylene cyanol), was added to 10 μl of the quenched reaction mixtures and heated to 70 °C for 2–5 min prior to loading 5 μl on a denaturing polyacrylamide gel of the appropriate percentage containing 1× TBE and 7 M urea. Highly cross-linked gels contained 1.7% bisacrylamide. Electrophoresis was performed in 1× TBE at 75 watts. Gels were visualized by using a PhosphorImager and quantitated by using the ImageQuant software (Molecular Dynamics). Data were fit by nonlinear regression using the program, KaleidaGraph (Synergy Software, Reading, PA).

Kinetic Simulation—Kinetic simulations were performed by using KinTekSim version 2.03 (KinTek Corp., State College, PA). All rate constants were determined experimentally, except where noted. The agreement between the experimental data and kinetic simulations was determined by visual inspection.

RESULTS

A Symmetrical Primer-Template Substrate (sym/sub) to Study 3D^{pol}-catalyzed Nucleotide Incorporation—We designed the symmetrical, heteropolymeric RNA primer-template substrate shown in Fig. 1*A* to study the kinetics and mechanism of 3D^{pol}-catalyzed nucleotide incorporation. We refer to this substrate as "sym/sub" throughout. This substrate is a 10-nt, self-complementary RNA that forms a 6-base pair duplex flanked by two, 4-nt 5′-overhangs. Each overhang is capable of templating incorporation of a unique nucleotide, thus permitting the evaluation of single and multiple cycles of nucleotide incorporation. The calculated T_m value is 55 °C for this duplex when 1 μM RNA strands (0.5 μM duplex) is employed (33). Based upon previous studies of 3D^{pol}, this T_m value is in the optimal range for maximal rates of nucleotide incorporation (34).

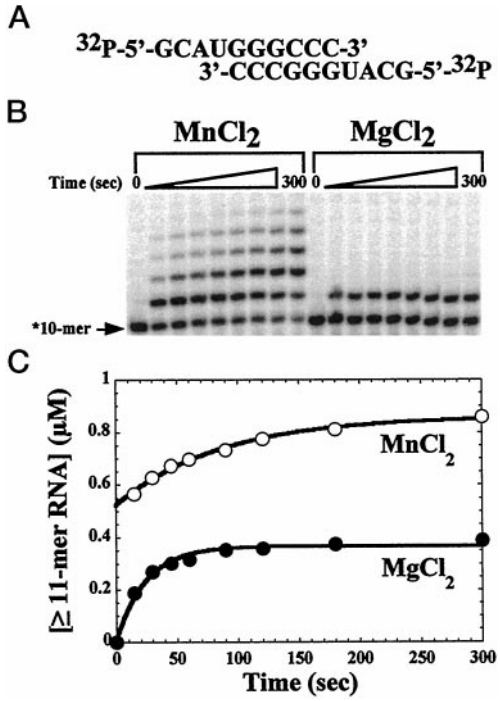

FIG. 1. **Use of a symmetrical primer-template (sym/sub) to study 3D^{pol}-catalyzed nucleotide incorporation.** *A,* sym/sub. *B,* AMP incorporation into sym/sub. Reactions contained 5 μM 3D^{pol}, 1 μM sym/sub (0.5 μM duplex), 500 μM ATP, and 5 mM $MnCl_2$ or $MgCl_2$. Reactions were initiated by addition of 3D^{pol} and incubated at 30 °C; reactions were quenched at the indicated times by addition of EDTA to a final concentration of 50 mM. Products were resolved by electrophoresis on a denaturing 20% polyacrylamide gel. *C,* kinetics of AMP incorporation into sym/sub in the reactions described in *B*, in the presence of either $MnCl_2$ (○) or $MgCl_2$ (●). The kinetics of AMP incorporation in the presence of $MgCl_2$ fit best to a single exponential (*solid line*) with an observed rate of 0.041 ± 0.004 s^{-1} and an amplitude of 0.36 ± 0.02 μM. The kinetics of AMP incorporation in the presence of $MnCl_2$ fit best to a single exponential (*solid line*) with an observed rate of 0.012 ± 0.001 s^{-1}, an amplitude of 0.34 ± 0.01 μM, and a starting point of 0.52 ± 0.02 μM.

Incorporation of the First Nucleotide into sym/sub by 3D^{pol} Is Slow—Utilization of sym/sub by 3D^{pol} is shown in Fig. 1*B*. In this experiment, enzyme was in excess (5 μM) relative to sym/sub (0.5 μM duplex); ATP (500 μM) was supplied as the sole nucleotide substrate; and either Mn^{2+} or Mg^{2+} was employed as divalent cation cofactor. In the presence of both divalent cations, AMP incorporation into sym/sub was observed. AMP incorporation was very error-prone in the presence of Mn^{2+} but very specific in the presence of Mg^{2+}. Quantitative evaluation of the kinetics of AMP incorporation into sym/sub showed that in the presence of Mn^{2+}, incorporation was biphasic. During the first phase, 0.52 ± 0.02 μM sym/sub was utilized at a rate too fast to measure by quenching the reaction manually. During the second phase, an additional 0.34 ± 0.04 μM sym/sub was utilized at a rate of 0.012 ± 0.001 s^{-1}. It should be noted that in order to extend greater than 0.5 μM RNA strands, the "flip side" of an extended sym/sub duplex must be utilized, thus mandating dissociation of a previously existing 3D^{pol}-sym/sub product complex. In the presence of Mg^{2+}, AMP incorporation into sym/sub was monophasic; 0.36 ± 0.02 μM sym/sub was

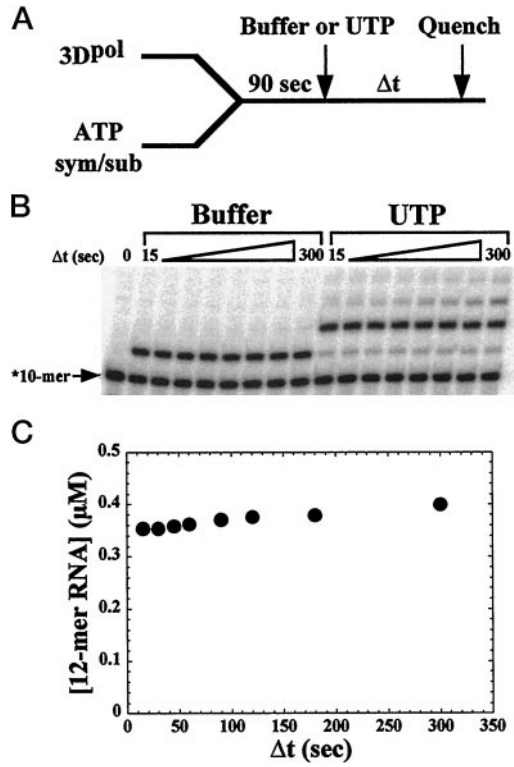

FIG. 2. **UMP incorporation into sym/sub.** *A,* experimental design. Reactions were initiated by mixing 3D^{pol} (5 μM) with sym/sub (1 μM), ATP (500 μM), and $MgCl_2$ (5 mM) and incubated at 30 °C for 90 s at which time either buffer or UTP (500 μM) was added. Reactions proceeded for indicated times then quenched by addition of EDTA (50 mM). *B,* products from reactions described in *A* resolved by electrophoresis on a denaturing 20% polyacrylamide gel. *C,* kinetics of UMP incorporation into sym/sub in the reaction described in *A*.

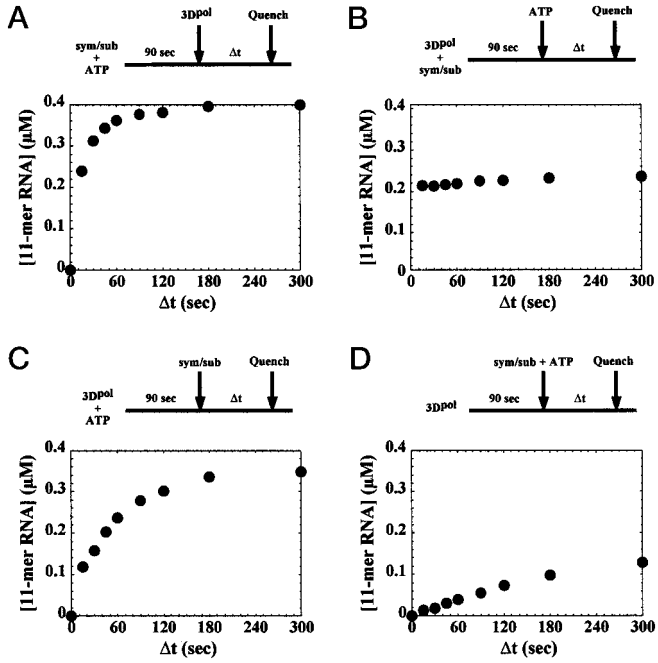

FIG. 3. **Order of addition.** Reactions contained 5 μM 3D^{pol}, 1 μM sym/sub (0.5 μM duplex), 500 μM ATP, and 5 mM $MgCl_2$. *A,* sym/sub and ATP were incubated at 30 °C for 90 s, at which time 3D^{pol} was added to initiate the reaction. Reactions were quenched at the indicated times by addition of EDTA (50 mM). The kinetics of AMP incorporation could be fit to a single exponential with an observed rate of 0.06 s^{-1} and an amplitude of 0.38 μM. *B,* 3D^{pol} and sym/sub were incubated at 30 °C for 90 s, at which time ATP was added to initiate the reaction. Reactions were quenched at the indicated times by addition of EDTA (50 mM). *C,* 3D^{pol} and ATP were incubated at 30 °C for 90 s, at which time sym/sub was added to initiate the reaction; the reaction was quenched at the indicated times by addition of EDTA (50 mM). The kinetics of AMP incorporation could be fit to a single exponential with an observed rate of 0.02 s^{-1} and an amplitude of 0.33 μM. *D,* 3D^{pol} was incubated at 30 °C for 90 s, at which time sym/sub and ATP were added to initiate the reaction. Reactions were quenched at the indicated times by addition of EDTA (50 mM). The kinetics of AMP incorporation could be fit to a single exponential with an observed rate of 0.004 s^{-1} and an amplitude of 0.18 μM.

extended at a rate of 0.041 ± 0.004 s^{-1}. The measured value of extended sym/sub (0.36 μM) was lower than the theoretical value (0.5 μM) for a single, stoichiometric turnover.

Incorporation of the Second Nucleotide into sym/sub by 3D^{pol} Is Fast—If the slow observed rate of nucleotide incorporation in the presence of Mg^{2+} reflected the true rate of 3D^{pol}-catalyzed nucleotide incorporation, then each subsequent cycle of incorporation should occur at approximately the same rate. However, if the true rate of incorporation was masked by the slow assembly of 3D^{pol}-sym/sub complexes, then each subsequent cycle of nucleotide incorporation may be faster. In order to address this issue, an experiment was performed in which 3D^{pol}, sym/sub, and ATP were incubated at 30 °C for 90 s, a time sufficient to accumulate 97% of the total possible 11-mer product (Fig. 2*A*). At this point, either buffer was added as a control for misincorporation, or the second nucleotide, UTP, was added (Fig. 2*A*). The kinetics of 11-mer conversion to 12-mer product were monitored from 15 s to 5 min. During the 5-min incubation period in the absence of UTP, misincorporation of AMP to form 12-mer product was not observed (Fig. 2*B, panel Buffer*). However, in less than 15 s, 94% of 11-mer was converted to products 12–14-nt in length in the presence of UTP (Fig. 2*B, panel UTP*; Fig. 2*C*). Products of misincorporation represented 6% of the total product at 15 s and increased linearly to 27% of the total product during the 5-min reaction time. These data are consistent with a model in which assembly of reactive ternary complexes limits the rate of single nucleotide incorporation when reactions are initiated by addition of 3D^{pol}.

Assembly of 3D^{pol}-sym/sub Complexes Prior to Addition of the First Nucleotide Results in Fast Incorporation—In order to determine whether a preferred order of assembly existed, the experiment shown in Fig. 3 was performed. In each experiment, the final concentrations of 3D^{pol} (5 μM), sym/sub (0.5 μM duplex), and ATP (500 μM) remained constant. The only difference was in the order of mixing/incubation at 30 °C. The results from a reaction initiated by addition of enzyme (Fig. 3*A*) were consistent with the analysis presented in Fig. 1 (k_{obs} was 0.06 ± 0.01 s^{-1}; amplitude was 0.38 ± 0.01 μM). Incubation of 3D^{pol} with sym/sub for 90 s prior to addition of ATP (Fig. 3*B*) completely removed the slow rate of incorporation. However, a 2-fold reduction in the amplitude (0.21 μM) was noted. Incubation of 3D^{pol} and ATP prior to addition of sym/sub (Fig. 3*C*) reduced the observed rate of AMP incorporation by 3-fold (k_{obs} was 0.02 s^{-1}) with very little effect on the end point of the reaction (amplitude was 0.33 μM). Incubation of 3D^{pol} at 30 °C prior to addition of sym/sub and ATP (Fig. 3*D*) showed significant thermal inactivation of 3D^{pol}.

Stability of 3D^{pol}—Thermal inactivation of 3D^{pol} will contribute significantly to the outcome of kinetic experiments performed with this enzyme; therefore, a rigorous analysis of this reaction was performed. In the presence of 20% glycerol, 3D^{pol} was stable for at least 1 week at temperatures less than or equal to 4 °C (data not shown). When frozen in glycerol-containing buffer at −80 °C, the enzyme was stable indefinitely and lost less than 10% activity after a single cycle of freezing and thawing (data not shown). However, upon dilution of 3D^{pol}

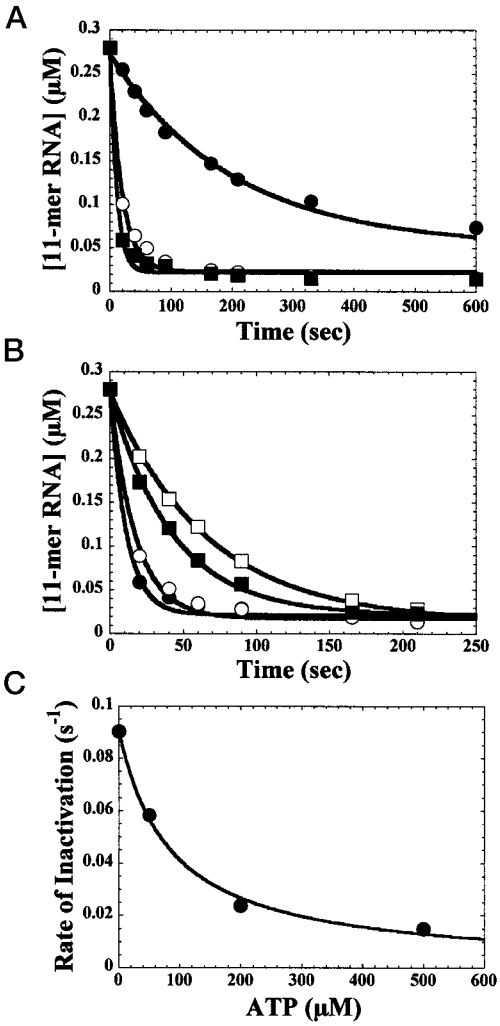

FIG. 4. **Inactivation of 3D^{pol}.** *A,* rate of 3D^{pol} inactivation is temperature-dependent. 3D^{pol} (2 μM) was incubated at 0 °C (●), 22 °C (○), or 30 °C (■) in 1× reaction buffer (50 mM HEPES, pH 7.5, 10 mM 2-mercaptoethanol, 60 μM $ZnCl_2$, and 5 mM $MgCl_2$), and at the indicated times the reaction was initiated by addition of sym/sub (1 μM) and ATP (500 μM) and allowed to proceed for an additional 90 s at 30 °C at which time the reaction was quenched by addition of EDTA (50 mM). The *solid lines* represent the fit of the data to a single exponential to give a $k_{inact(obs)}$ at 0, 22, and 30 °C of 0.0005 ± 0.00005, 0.051 ± 0.005, and 0.090 ± 0.011 s^{-1}, respectively. *B,* ATP protects 3D^{pol} against inactivation. 3D^{pol} (2 μM) was incubated with 0 (●), 50 (○), 200 (■), or 500 (□) μM ATP at 30 °C, and at the indicated times the reaction was initiated by addition of sym/sub (1 μM) and ATP (500 μM final) and allowed to proceed for an additional 90 s at which time the reaction was quenched by addition of EDTA (50 mM). The *solid lines* represent the fit of the data to a single exponential to give a $k_{inact(obs)}$ at 0, 50, 200, and 500 μM ATP of 0.090 ± 0.011, 0.058 ± 0.005, 0.024 ± 0.001, and 0.015 ± 0.001 s^{-1}, respectively. *C,* protection by ATP is saturable. The observed rate of inactivation of 3D^{pol} measured at 30 °C described in *B* was plotted as a function a ATP concentration, and the data were fit (*solid line*) to the following equation: $k_{inact(obs)} = k_{inact(max)} - ((k_{inact(max)}*[ATP])/(K_{0.5(ATP)} + [ATP]))$. The $k_{inact(max)}$ was 0.091 ± 0.003 s^{-1} and the $K_{0.5(ATP)}$ was 83.6 ± 9.2 μM.

into our standard reaction buffer which lacks glycerol (see "Experimental Procedures"), 3D^{pol} activity was lost at a finite rate at temperatures greater than or equal to 0 °C (Fig. 4*A*). Consistent with previous results (35), nucleotide, in this case ATP, protected 3D^{pol} against inactivation (Fig. 4*B*). Protection of 3D^{pol} by ATP was apparent at all temperatures analyzed (Table I) and was saturable (Fig. 4*C* and Table II). The maximal rates of inactivation varied over a 20-fold range between 0 and 30 °C. Interestingly, the concentration of ATP sufficient to decrease the observed rate of inactivation to 50% of the maximal value ($K_{0.5(ATP)}$) also showed a temperature dependence, ranging from 17 μM at 0 °C to 84 μM at 30 °C. In addition to ATP, GTP, GDP, UTP, and CTP were also capable of protecting 3D^{pol} against thermal inactivation (Fig. 5). As observed previously, GTP protects 3D^{pol} against thermal inactivation better than any other nucleotide (35). We also noted a linear, 3-fold decrease in $k_{inact(max)}$ when the concentration of 3D^{pol} was varied between 2 and 20 μM (data not shown).

TABLE I
Comparison of 3D^{pol} inactivation rates as a function of temperature and ATP concentration

Experiments were performed as described in the legend to Fig. 4, *A* and *B*.

[ATP]	0 °C	22 °C	30 °C
μM	(× 10^{-3}) s^{-1}	(× 10^{-3}) s^{-1}	(× 10^{-3}) s^{-1}
0	5.0 ± 0.5	51.0 ± 5.0	90.0 ± 11.0
50	1.3 ± 0.1	21.0 ± 2.0	58.0 ± 5.0
200	0.31 ± 0.02	8.5 ± 0.9	24.0 ± 1.0
500	0.16 ± 0.01	4.8 ± 1.5	15.0 ± 1.0

TABLE II
Temperature dependence of constants for inactivation of 3D^{pol}

Parameters were obtained as described in the legend to Fig. 4*C*.

Parameter	0 °C	22 °C	30 °C
$k_{inact(max)}$ (s^{-1})	0.0050 ± 0.0001	0.051 ± 0.001	0.091 ± 0.003
$K_{0.5(ATP)}$ (μM)	17.0 ± 1.1	37.0 ± 3.1	83.6 ± 9.2

Stability of 3D^{pol}-sym/sub Complexes—Although the rate of formation of the initial 3D^{pol}-sym/sub complex was slow, this complex was stable enough to incorporate quantitatively the second nucleotide. In order to determine directly the rate constant for dissociation of this complex, we performed the experiment that is illustrated in Fig. 6*A*. 3D^{pol} and 5′-^{32}P-labeled sym/sub were given 90 s to assemble, at which point a 1000-fold molar excess of unlabeled sym/sub was added as a trap for free enzyme. At various times after addition of trap, the amount of complex remaining was determined by following production of 11-mer (Fig. 6*B*). At 30 °C, the 3D^{pol}-sym/sub complex had a half-life of ~20 min, whereas at 22 °C, this complex had a half-life of ~2 h (Fig. 6*C*). A similar experiment was performed to determine the stability of the 3D^{pol}-sym/sub product complex (Fig. 6*D*); however, in this case, the ability to form 12-mer was monitored (Fig. 6*E*). Again, there was a temperature dependence to the stability of this complex (Fig. 6*F*). The product complexes had half-lives of 4.5 and 8.5 h at 30 and 22 °C, respectively.

Kinetics of Ribo- and Deoxyribonucleotide Incorporation by 3D^{pol}—By using a rapid mixing/quenching device, we were able to evaluate the kinetics of AMP incorporation into sym/sub from preassembled 3D^{pol}-sym/sub complexes (Fig. 7). In the presence of 600 μM ATP, incorporation of AMP was fast, occurring at a rate of ~70 s^{-1}. Under the same conditions, both 2′-dAMP and 3′-dAMP were also incorporated, albeit at rates 70–120-fold slower than for AMP (Table III). The loss of each hydroxyl appeared to be additive as incorporation of 2′,3′-ddAMP was reduced by 35,000-fold relative to AMP incorporation (Table III).

Steady-state kinetic analysis of AMP incorporation into sym/sub showed a burst of product formation followed by a linear accumulation of product (Fig. 8). The steady-state rate constant, k_{cat}, for AMP incorporation was 0.0001 s^{-1}, and the *y* intercept was 0.8 μM. In the presence of all four NTPs, the k_{cat} value was increased by 10-fold relative to that in the presence of ATP only (Fig. 8). There was not a significant difference in the *y* intercept (Fig. 8). The k_{cat} value for AMP incorporation did not change by increasing the concentration of 3D^{pol} to 2.5

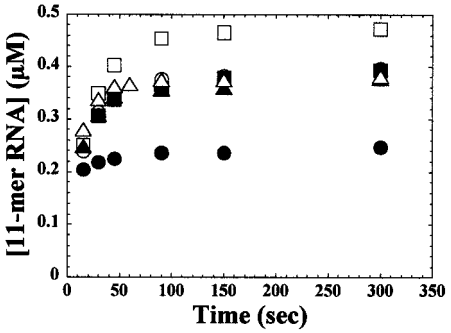

FIG. 5. **Incorrect nucleotides and nucleoside diphosphates protect 3D^{pol} against inactivation.** Reactions contained 5 μM 3D^{pol}, 1 μM sym/sub (0.5 μM duplex), 5 mM $MgCl_2$, 50 μM ATP, and either 0 μM ATP (●), 450 μM ATP (○), 450 μM CTP (■), 450 μM GTP (□), 450 μM UTP (▲), or 450 μM GDP (△). Reactions were initiated by addition of 3D^{pol} and incubated at 30 °C; reactions were quenched at the indicated times by addition of EDTA to a final concentration of 50 mM.

μM; the *y* intercept was 2.0 μM (data not shown).

Kinetic Mechanism for Assembly of Stable, Elongation-competent 3D^{pol}-sym/sub Complexes—In order to understand better the kinetic mechanism for assembly of 3D^{pol}-sym/sub complexes, we evaluated the kinetics of assembly indirectly by monitoring AMP incorporation into sym/sub under conditions in which either the concentration of 3D^{pol} or sym/sub was varied. The results of this analysis are presented in Fig. 9. The data were most consistent with the mechanism presented in Scheme 1. The validity of this model was tested by kinetic simulation of this mechanism using the parameters shown in Table IV. The simulated data are represented by the *solid lines* through the data shown in Fig. 9. The concentration of active 3D^{pol} (0.8 μM) was from the *y* intercept of the steady-state kinetic data (Fig. 8). A K_d value for ATP of 100 μM was employed.[2] This value is consistent with reported K_m values for nucleotides (30). This K_d value was inconsequential to the outcome of the simulation as this value could be varied by an order of magnitude in either direction without any effect on the simulated kinetics of assembly. The rate constant for the conformational change was constrained by the observed rate of assembly at 5 and 10 μM sym/sub. A value of 0.076 s^{-1} was obtained from a single exponential fit of these individual time courses. Therefore, the only simulated parameters were k_{+1} and k_{-1}. Given the constraints discussed above, values of 0.1 μM^{-1} s^{-1} and 0.1 s^{-1} for k_{+1} and k_{-1}, respectively, were shown to fit the data best. The simulated data were quite sensitive to these rate constants as a 25% change in either altered the goodness of fit to the data. A good fit of the data acquired by varying 3D^{pol} concentration was obtained only when the fraction of inactive enzyme (20% of the total upon initiation) was allowed to bind to sym/sub. This unproductive complex was kinetically significant at all concentrations of 3D^{pol}, even more so at low concentrations of sym/sub ($\leq$1 μM). At 30 °C in the presence of sym/sub and absence of glycerol, 3D^{pol} concentrations in the 10–25 μM range showed evidence of precipitation; therefore, these data were not included in the analysis. Given this problem with precipitation, we did not force a fit of the mechanism to the 5 μM 3D^{pol} data (Fig. 9*A*). It should be noted, however, that at 5 μM 3D^{pol} we were unable to observe any precipitation even after centrifugation.

DISCUSSION -

We have used a symmetrical primer-template substrate (sym/sub) to assemble stable, elongation-competent 3D^{pol}-sym/sub complexes suitable for analysis of the kinetics and mechanism of nucleotide incorporation catalyzed by this enzyme. Our current model for the mechanism of 3D^{pol}-sym/sub complex assembly is presented in Scheme 1. 3D^{pol} undergoes iterative cycles of binding and release of sym/sub until the complex isomerizes into a catalytically competent elongation complex. After each cycle of dissociation, enzyme inactivation can occur. 3D^{pol} inactivation results in substoichiometric assembly of elongation complexes. The fraction of enzyme that will be inactivated during the assembly process depends upon the partitioning between the two pathways. Maximizing the rate of 3D^{pol}-sym/sub complex formation and minimizing the rate of 3D^{pol} inactivation will permit stoichiometric assembly of elongation complexes. By using concentrations of sym/sub in a range greater than or equal to 10 μM, the rate of assembly will be maximized (Fig. 9*B*). By assembling complexes at lower temperatures in the presence of nucleotide, the rate of 3D^{pol} inactivation will be minimized (Fig. 4). It may also be possible to assemble complexes efficiently by using Mn^{2+} as the divalent cation cofactor and then diluting these mixtures into Mg^{2+}-containing buffer to prevent error-prone RNA synthesis (Fig. 1 and Ref. 30). Once complexes form, they are very stable (Fig. 6*A*), support a fast rate of nucleotide incorporation (Fig. 7), and produce complexes that are significantly more stable than the initial complex (Fig. 6*B*). The rate of complex disassembly limits the rate of primer utilization (Fig. 8). The rate of complex disassembly is faster from the end of template than from internal positions (Fig. 8). Therefore, the number of primers utilized during the course of a reaction can be increased by following incorporation of all four nucleotides instead of a single nucleotide.

We were also able to fit the data by using an alternative model with a slow association step without a conformational change step. In this case, the rate constant for association was 0.035 μM^{-1} s^{-1}, and the rate constant for dissociation was that measured directly, 0.0006 s^{-1} (Fig. 6). However, in order to obtain a good fit, it was necessary to reduce artificially the concentration of sym/sub employed from 0.5 to 0.4 μM. We observe stoichiometric (0.5 μM) utilization of sym/sub in the presence of Mn^{2+} (Fig. 1*C*). This observation confirms that all of the substrate is competent for primer extension. Kinetic simulation should always be constrained by parameters determined empirically. Therefore, this model was not considered further. Attempts were also made to add a monomer-oligomer equilibrium to the mechanism in order to fit the kinetics of assembly in the presence of excess (5 μM) 3D^{pol} (Fig. 9*A*). These attempts failed owing to the lack of empirical data (and corresponding constraints) to describe this reaction. Direct analysis of 3D^{pol} oligomerization should provide information necessary to explore this possibility more rigorously.

Whether the mechanism of assembly described herein can be related to initiation of transcription or replication *in vivo* remains to be determined. These studies employ an artificial primer-template; therefore, the kinetic scheme and associated parameters may only be relevant for the model system. The kinetic properties may be different for a reaction of the polymerase with a natural template in the presence of other protein factors. Replication of the poliovirus genome initiates within the poly(A)-tract at the 3′-end of genomic RNA from a complex comprising viral factors 3AB, 3B (VPg), 3CD, and 3D^{pol} (Fig. 10) (36). Once 3D^{pol} initiates RNA synthesis from the protein primer, an elongation-competent complex is formed. As indicated in Fig. 10, a single template is thought to support multiple, continuous cycles of initiation. The nascent RNA chain is only annealed to template over a short distance, and the RNA is spooled through a channel formed by the polymerase (37). Whether or not a helicase is required to disrupt base pairing

[2] J. J. Arnold and C. E. Cameron, unpublished results.

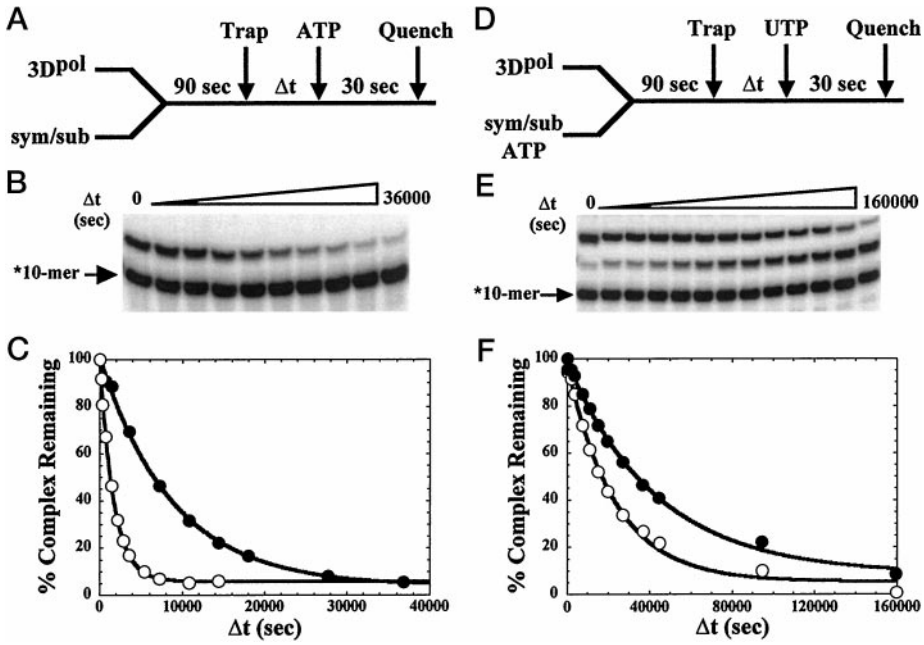

FIG. 6. **Dissociation of 3D^{pol}-sym/sub and 3D^{pol}-sym/sub product complexes.** *A,* experimental design. 3D^{pol} (1 μM) was incubated with 100% labeled sym/sub (0.1 μM) for 90 s at either 22 or 30 °C at which point trap (100 μM unlabeled sym/sub) was added to the reaction. At fixed times after the addition of trap, ATP (500 μM) was added, and the reaction was allowed to proceed for 30 s and then quenched by addition of EDTA (50 mM). *B,* products from reactions described in *A* performed at 22 °C resolved by electrophoresis on a denaturing highly cross-linked 23% polyacrylamide gel. *C,* kinetics of dissociation of 3D^{pol}-sym/sub complexes from the reactions described in *A* at 22 °C (●) and 30 °C (○). The *solid lines* represent the fit of the data to a single exponential and gives a k_{obs} at 22 and 30 °C of 0.00011 ± 0.000005 and 0.00059 ± 0.00002 s^{-1}, respectively. *D,* experimental design. 3D^{pol} (1 μM) was incubated with 100% labeled sym/sub (0.1 μM) and ATP (1 μM) for 90 s at either 22 or 30 °C at which point trap (100 μM unlabeled sym/sub) was added to the reaction. At fixed times after the addition of trap, UTP (500 μM) was added, and the reaction was allowed to proceed for 30 s and then quenched by addition of EDTA (50 mM). *E,* products from reactions described in *D* performed at 22 °C resolved by electrophoresis on a denaturing, highly cross-linked 23% polyacrylamide gel. *F,* kinetics of dissociation of 3D^{pol}-sym/sub product complexes from the reactions described in *D* at 22 (●) and 30 °C (○). The *solid lines* represent the fit of the data to a single exponential and gives a k_{obs} at 22 and 30 °C of 0.000023 ± 0.000001 and 0.000043 ± 0.000003 s^{-1}, respectively.

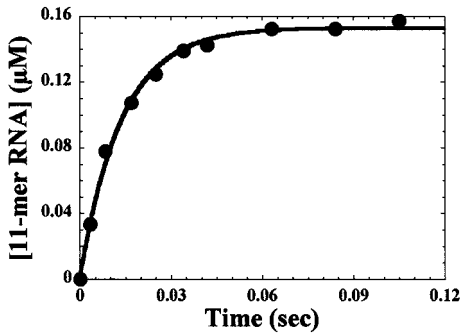

FIG. 7. **Pre-steady-state incorporation of AMP into sym/sub.** 2 μM 3D^{pol} was incubated with 2 μM sym/sub (1 μM duplex) and rapidly mixed with 1200 μM ATP as described under "Experimental Procedures." After mixing, reactant concentrations were reduced by 50%. Reactions were quenched at the indicated times by addition of 0.5 M EDTA to a final concentration of 0.3 M. The *solid line* represents the fit of the data to a single exponential with a k_{obs} of 72.4 ± 4.4 s^{-1}.

between template and nascent RNA is not known.

We hypothesize that 3D^{pol}-sym/sub complexes mimic complexes formed during elongation of poliovirus plus- and minus-strand RNAs by 3D^{pol} (Fig. 10). In support of this hypothesis is the observation that a 3D^{pol} derivative with an amino acid substitution in conserved structural motif B that has less than a 2-fold reduction in poly(rU) polymerase activity but a 15-fold reduction in the observed rate of elongation measured by using the sym/sub system produces virus with significantly impaired growth properties relative to wild-type virus.[3] Moreover, the rate of nucleotide incorporation into sym/sub and stability of

TABLE III
Rates of incorporation of ribo- and deoxyribonucleotides

Experiments were performed as described in the legend to Fig. 7 for AMP, 2′-dAMP, and 3′-dAMP incorporation. For 2′,3′-ddAMP incorporation, reactions were performed as follows. Reactions contained 5 μM 3D^{pol}, 1 μM sym/sub (0.5 μM duplex), 5 mM $MgCl_2$, and 500 μM 2′,3′-ddATP. Reactions were initiated by addition of 3D^{pol}, incubated at 30 °C, and quenched by addition of EDTA to a final concentration of 50 mM. The k_{obs} was obtained from the fit of the data to a single exponential.

Nucleotide	k_{obs}
	s^{-1}
ATP	72.4 ± 4.4
2′-dATP	0.596 ± 0.025
3′-dATP	0.928 ± 0.094
2′,3′-ddATP	0.0020 ± 0.0002

the 3D^{pol}-sym/sub complex predicts processive replication of the complete genome by a single polymerase molecule in approximately 100 s. This value is in agreement with the value of 45 s measured *in vivo* (37). As long as 3D^{pol} can proceed along the template unimpeded by RNA secondary structure, additional factors may not be required to assist in elongation.

Within infected cells, replication occurs in spherical compartments formed by virus-induced vesicles that are 0.5 μm in diameter (38). This diameter predicts a volume of 0.065 μm^3. Enclosure of as few as 10 RNA molecules within this structure would correspond to a concentration in the micromolar range. Nonstructural proteins, such as 3D^{pol}, are present in a 1:1 stoichiometry with structural proteins that are required in 60-fold molar excess of RNA for virion assembly (37). Therefore, the concentration of 3D^{pol} within replication complexes will also be in the micromolar range. However, metabolic labeling experiments have shown that in virus-infected cells the

[3] S. Crotty, J. J. Arnold, D. W. Gohara, R. Andino, and C. E. Cameron, unpublished observations.

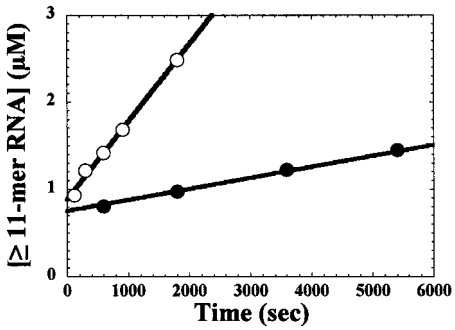

FIG. 8. **Steady-state incorporation of AMP and multiple nucleotides into sym/sub.** Reactions contained 20 μM sym/sub (10 μM duplex), 5 mM $MgCl_2$, 1 μM 3D^{pol}, and either 500 μM ATP (●) or 200 μM NTPs (○). Reactions were initiated by addition of 3D^{pol} and incubated at 30 °C; reactions were quenched at the indicated times by addition of EDTA to a final concentration of 50 mM. The *solid lines* represent the fit of the data to a line with a k_{cat} of 0.0001 ± 0.00001 and 0.001 ± 0.0001 s^{-1} for AMP and multiple nucleotide incorporation, respectively. The *y* intercept was 0.79 ± 0.06 μM for AMP incorporation and 0.87 ± 0.06 μM for multiple nucleotide incorporation.

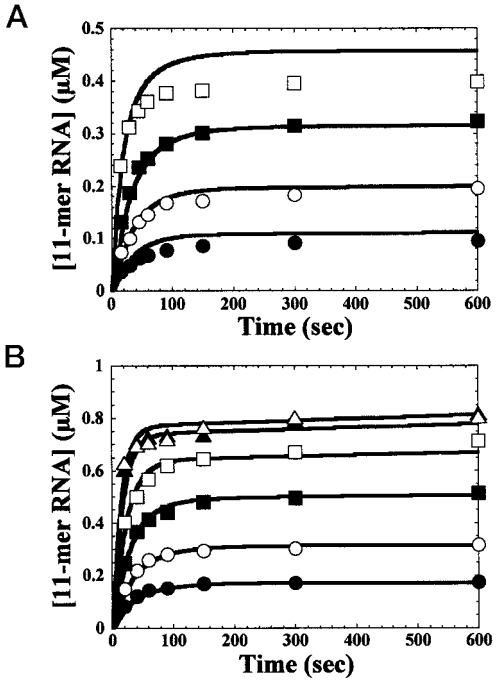

FIG. 9. **Kinetics of 3D^{pol}-catalyzed nucleotide incorporation.** *A,* concentration dependence of 3D^{pol}. Reactions contained 1 μM sym/sub (0.5 μM duplex), 500 μM ATP, 5 mM $MgCl_2$, and either 0.25 (●), 0.5 (○), 1 (■), or 5 (□) μM 3D^{pol}. Reactions were initiated by addition of 3D^{pol} and incubated at 30 °C; reactions were quenched at the indicated times by addition of EDTA to a final concentration of 50 mM. The *solid lines* represent the kinetic simulation of the mechanism shown in Scheme 1 with the kinetic parameters shown in Table IV. *B,* concentration dependence of sym/sub. Reactions contained 1 μM 3D^{pol}, 500 μM ATP, 5 mM $MgCl_2$, and either 0.25 (●), 0.5 (○), 1 (■), 2 (□), 5 (▲), or 10 (△) μM sym/sub (duplex). Reactions were initiated by addition of 3D^{pol} and incubated at 30 °C; reactions were quenched at the indicated times by addition of EDTA to a final concentration of 50 mM. The *solid lines* represent the kinetic simulation of the mechanism shown in Scheme 1 with the kinetic parameters shown in Table IV.

polymerase subunit can be found in precursor (P3 and 3CD) and processed forms (3D^{pol} and 3D′). 3D′ is a proteolytic fragment of 3D^{pol} that presumably lacks polymerase activity. The ratio of P3:3CD:3D^{pol}:3D′ is 2:4:1:1 after a 10-min labeling period, thus reducing the concentration of 3D^{pol} available for transcription and replication. We conclude that the concentration of sym/sub and 3D^{pol} employed in this study is in the biologically relevant range. In addition, the calculated K_d value

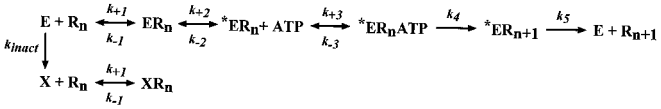

SCHEME 1. **Minimal kinetic mechanism for assembly of and nucleotide incorporation by 3D^{pol}-sym/sub complexes.** *E*(3D^{pol}); *X* (inactive 3D^{pol}); R_n (sym/sub); *ER_n (active elongation complex).

TABLE IV
Kinetic parameters for the mechanism of 3D^{pol}-sym/sub complex assembly (Scheme 1)

Parameter	Value[a]
k_{+1}	0.1 $\mu M^{-1}s^{-1}$
k_{-1}	0.1 s^{-1}
k_{+2}	0.076 s^{-1}
k_{-2}	0.0006 s^{-1}
k_{-3}/k_{+3}	100 μM[b]
k_4	72 s^{-1}[c]
k_5	0.0001 s^{-1}
k_{inact}	0.015 s^{-1}

[a] Values for all parameters, with the exception of k_{+1} and k_{-1}, were determined experimentally.
[b] See Footnote 2 and Ref. 30. Values ≤1000 μM were tolerated without any deviation in the fit of the stimulation to the data.
[c] Values ≥1 s^{-1} were tolerated without any deviation in the fit of the stimulation to the data.

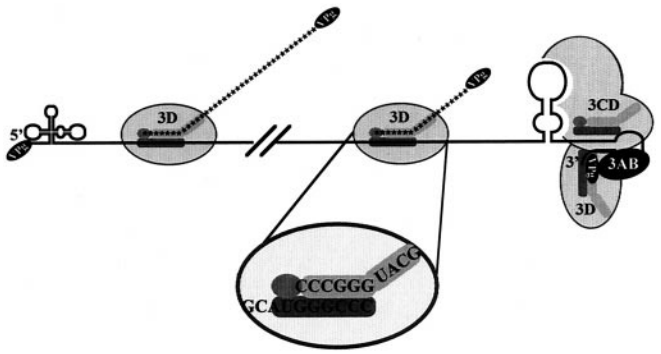

FIG. 10. **3D^{pol}-sym/sub complexes as a model for elongation complexes during poliovirus genome transcription and replication.** See text for details.

(k_{+1}/k_{-1}, Table IV) of 1 μM for sym/sub reported herein along with the micromolar K_m and K_d values for nucleic acid reported previously by us (30, 34) and others (39) are in a physiological range. Despite the fact that polymerase is present in excess of RNA and both are in the micromolar range, given an association rate constant of 0.1 μM^{-1} s^{-1}, it is possible that formation of the initial 3D^{pol}-sym/sub complex could be the rate-limiting step for initiation.

In vivo, the density of polymerase molecules on any template has been determined to be ~6–8 (37). If it takes 100 s for the polymerase to traverse the entire genome, then this would set a lower limit of 0.06–0.08 s^{-1} on the rate of initiation. This value is remarkably close to that measured for the rate of the conformational change step (0.076 s^{-1}) in our model for assembly. This conformational change after binding of sym/sub to 3D^{pol} may reflect repositioning of the primer strand into the "exit channel" for nascent RNA. Such reorganization could maximize polymerase-nucleic acid interactions. Indeed, this isomerization greatly enhances the stability of this complex; the rate constant for dissociation is decreased from 0.1 s^{-1} to 0.0006 s^{-1}. This difference corresponds to at least 5 kcal/mol, consistent with the formation of 5–10 hydrogen bonds. A conformational change upon complete occupancy of the polymerase nucleic acid-binding site by single-stranded RNA has also been proposed by Kirkegaard and colleagues (39). Perhaps a conformational change that positions the protein primer into the exit

channel limits and regulates the rate of initiation *in vivo.* An alternative possibility for the conformational change step observed kinetically comes from structural studies of the RdRP from hepatitis C virus (40). Extensive interactions between the fingers and thumb subdomains exist in this enzyme which completely encircle the catalytic center of the enzyme. Similar interactions should be possible for 3D^{pol}; therefore, the observed conformational change step may reflect "closing" of the enzyme. The increased stability of this complex would derive from the additional interactions between the fingers and thumb subdomains.

The steady-state kinetic experiments (Fig. 8) were performed by using excess sym/sub; therefore, the *y* intercept reflects the active concentration of enzyme used in the reaction. The value measured in all cases was 80% of the value expected based on the concentration determined by absorbance at 280 nm (31). The value of 80% was also corroborated by the assembly experiments shown in Fig. 9*B*. That 20% was inactive was supported by the necessity to consider this species in our modeling of the kinetics of assembly in reactions that vary 3D^{pol} concentration (Fig. 9*A*). Taken together, these data suggest that a 3D^{pol} monomer is an active form of the enzyme. Oligomerization of this enzyme clearly can occur in the presence and absence of nucleic acid (29, 39). Mutations in 3D^{pol}-coding sequence that are predicted to shift the monomer-oligomer equilibrium in favor of monomer render the virus inviable (41). Our data suggest that sym/sub binding to 3D^{pol} oligomers produces catalytically inactive complexes, thus precluding quantitative assembly of active complexes when a high concentration of 3D^{pol} is employed (Fig. 9*A*). In addition, it is possible that the inactive fraction (20%) observed at 1 μM 3D^{pol} may represent an oligomeric species. The role of 3D^{pol} oligomerization *in vivo* remains elusive and warrants continued investigation.

Consistent with previous results (30), 3D^{pol} incorporates 2′- and 3′-dNMPs (Table III). During the first cycle of incorporation, NTP/2′-dNTP selection is low (121-fold) relative to 2′-dNTP/NTP selection by Klenow fragment of DNA polymerase I (10^3-10^6-fold) from *Escherichia coli* (42) and reverse transcriptase (10^5-fold) from human immunodeficiency virus (7). However, NTP/2′-dNTP selection is similar to that observed for the DNA-dependent RNA polymerase (80-fold) from bacteriophage T7 (43). Incorporation of 2′-dNMPs *in vivo* should be minimized by the low cytosolic availability of dNTPs relative to rNTPs. Of course, active mechanisms that preclude single and/or multiple cycles of dNMP incorporation cannot be ruled out at this time (30). Whether the observed NTP/2′-dNTP selection is a ground state, transition state, or combined effect requires another study but can be determined by using the sym/sub system. In addition, elucidation of the structural basis for NTP/dNTP selection should be facilitated by using the sym/sub system.

The use of the sym/sub system to study 3D^{pol} will advance our understanding of the RdRP to the level of the other classes of nucleic acid polymerase. The sym/sub system should be useful for the analysis of other RdRPs, especially members of the supergroup I family (44). We have used this substrate to identify and characterize the active form of the feline calicivirus polymerase.[4] In contrast, the RdRPs from bovine viral diarrhea virus and hepatitis C virus, members of the supergroup II family (44), do not assemble stable, elongation-competent complexes by using sym/sub.[2] Whether a universal primer-template design exists that is suitable for mechanistic analysis of all RdRPs remains to be determined.

Acknowledgments—We thank Raul Andino, Shane Crotty, Aniko Paul, and Kevin Raney for comments on the manuscript.

[4] L. Wei, K. Green, and C. E. Cameron, unpublished results.

REFERENCES

1. Elion, G. B. (1983) *J. Antimicrob. Chemother.* **12,** Suppl. B, 9–17
2. De Clercq, E. (1994) *Ann. N. Y. Acad. Sci.* **724,** 438–456
3. Reardon, J. E. (1992) *Biochemistry* **31,** 4473–4479
4. Reardon, J. E. (1993) *J. Biol. Chem.* **268,** 8743–8751
5. Kati, W. M., Johnson, K. A., Jerva, L. F., and Anderson, K. S. (1992) *J. Biol. Chem.* **267,** 25988–25997
6. Hsieh, J.-C., Zinnen, S., and Modrich, P. (1993) *J. Biol. Chem.* **268,** 24607–24613
7. Zinnen, S., Hsieh, J.-C., and Modrich, P. (1994) *J. Biol. Chem.* **269,** 24195–24202
8. Lanchy, J.-M., Ehresmann, C., Le Grice, S. F. J., Ehresmann, B., and Marquet, R. (1996) *EMBO J.* **15,** 7178–7187
9. Spence, R. A., Kati, W. M., Anderson, K. S., and Johnson, K. A. (1995) *Science* **267,** 988–993
10. Spence, R. A., Anderson, K. S., and Johnson, K. A. (1996) *Biochemistry* **35,** 1054–1063
11. Kerr, S. G., and Anderson, K. S. (1997) *Biochemistry* **36,** 14064–14070
12. Feng, J. Y., and Anderson, K. S. (1999) *Biochemistry* **5,** 55–63
13. Kohlstaedt, L. A., Wang, J., Friedman, J. M., Rice, P. A., and Steitz, T. A. (1992) *Science* **256,** 1783–1790
14. Jacobo-Molina, A., Ding, J., Nanni, R. G., Clark, A. D., Jr., Lu, X., Tantillo, C., Williams, R. L., Kamer, G., Ferris, A. L., Clark, P., Hizi, A., Hughes, S. H., and Arnold, E. (1993) *Proc. Natl. Acad. Sci. U. S. A.* **90,** 6320–6324
15. Ren, J. S., Esnouf, R., Hopkins, A., Ross, C., Jones, Y., Stammers, D., and Stuart, D. (1995) *Nat. Struct. Biol.* **2,** 293–302
16. Ensouf, R., Ren, J., Ross, R., Jones, Y., Stammers, D., and Stuart, D. (1995) *Nat. Struct. Biol.* **2,** 303–308
17. Rodgers, D. W., Gamblin, S. J., Harris, B. A., Ray, S., Culp, J. S., Hellmig, B., Woolf, D. J., Debouck, C., Harrison, S. C. (1995) *Proc. Natl. Acad. Sci. U. S. A.* **92,** 1222–1226
18. Huang, H., Chopra, R., Verdine, G. L., and Harrison, S. C. (1998) *Science* **282,** 1669–1675
19. Ollis, D. L., Brick, P., Hamlin, R., Xuong, N. G., and Steitz, T. A. (1985) *Nature* **313,** 762–766
20. Sousa, R., Chung, Y. J., Rose, J. P., and Wang, B. C. (1993) *Nature* **364,** 593–599
21. Wang, J., Sattar, A. K., Wang, C. C., Karam, J. D., Konigsberg, W. H., and Steitz, T. A. (1997) *Cell* **89,** 1087–1099
22. Doublié, S., Tabor, S., Long, A. M., Richardson, C. C., and Ellenberger, T. (1998) *Nature* **391,** 251–258
23. Kiefer, J. R., Mao, C., Braman, J. C., and Beese, L. S. (1998) *Nature* **391,** 304–307
24. Li, Y., Korolev, S., and Waksman, G. (1998) *EMBO J.* **17,** 7514–7525
25. Benkovic, S. J., and Cameron, C. E. (1995) *Methods Enzymol.* **262,** 257–269
26. Patel, S. S., Wong, I., and Johnson, K. A. (1991) *Biochemistry* **30,** 511–525
27. Capson, T. L., Peliska, J. A., Kaboord, B. F., Frey, M. W., Lively, C., Dahlberg, M., and Benkovic, S. J. (1992) *Biochemistry* **31,** 10984–10994
28. Jia, Y., and Patel, S. S. (1997) *Biochemistry* **36,** 4223–4232
29. Hansen, J. L., Long, A. M., and Schultz, S. C. (1997) *Structure* **5,** 1109–1122
30. Arnold, J. J., Ghosh, S. K. B., and Cameron, C. E. (1999) *J. Biol. Chem.* **274,** 37060–37069
31. Gohara, D. W., Ha, C. S., Ghosh, S. K. B., Arnold, J. J., Wisniewski, T. J., and Cameron, C. E. (1999) *Protein Expression Purif.* **17,** 128–138
32. Carroll, S. S., Benseler, F., and Olsen, D. B. (1996) *Methods Enzymol.* **275,** 365–382
33. Serra, M. J., and Turner, D. H. (1995) *Methods Enzymol.* **259,** 242–261
34. Arnold, J. J., and Cameron, C. E. (1999) *J. Biol. Chem.* **274,** 2706–2716
35. Richards, O. C., Yu, P., Neufeld, K. L., and Ehrenfeld, E. (1992) *J. Biol. Chem.* **267,** 17141–17146
36. Paul, A. V., van Boom, J. H., Filippov, D., and Wimmer, E. (1998) *Nature* **393,** 280–284
37. Rueckert, R. R. (1996) in *Fields Virology* (Fields, B. N., Knipe, D. M., and Howley, P. M., eds) Vol. 1, pp. 609–654, Lippincott-Raven Publishers, Philadelphia
38. Bolten, R., Egger, D., Gosert, R., Schaub, G., Landmann, L., and Bienz, K. (1998) *J. Virol.* **72,** 8578–8585
39. Beckman, M. T. L., and Kirkegaard, K. (1998) *J. Biol. Chem.* **273,** 6724–6730
40. Lesburg, C. A., Cable, M. B., Ferrrari, E., Hong, Z., Mannarino, A. F., and Weber, P. C. (1999) *Nat. Struct. Biol.* **6,** 937–943
41. Diamond, S. E., and Kirkegaard, K. (1994) *J. Virol.* **68,** 863–876
42. Astatke, M., Ng, K., Grindley, N. D. F., and Joyce, C. M. (1998) *Proc. Natl. Acad. Sci. U. S. A.* **95,** 3402–3407
43. Huang, Y., Eckstein, F., Padilla, R., and Sousa, R. (1997) *Biochemistry* **36,** 8231–8242
44. Koonin, E. V. (1991) *J. Gen. Virol.* **72,** 2197–2206

Poliovirus RNA-dependent RNA Polymerase ($3D^{pol}$): ASSEMBLY OF STABLE, ELONGATION-COMPETENT COMPLEXES BY USING A SYMMETRICAL PRIMER-TEMPLATE SUBSTRATE (sym/sub)

Jamie J. Arnold and Craig E. Cameron

J. Biol. Chem. 2000, 275:5329-5336.
doi: 10.1074/jbc.275.8.5329
